Institute of Paper Science and Technology
Atlanta, Georgia

IPST TECHNICAL PAPER SERIES

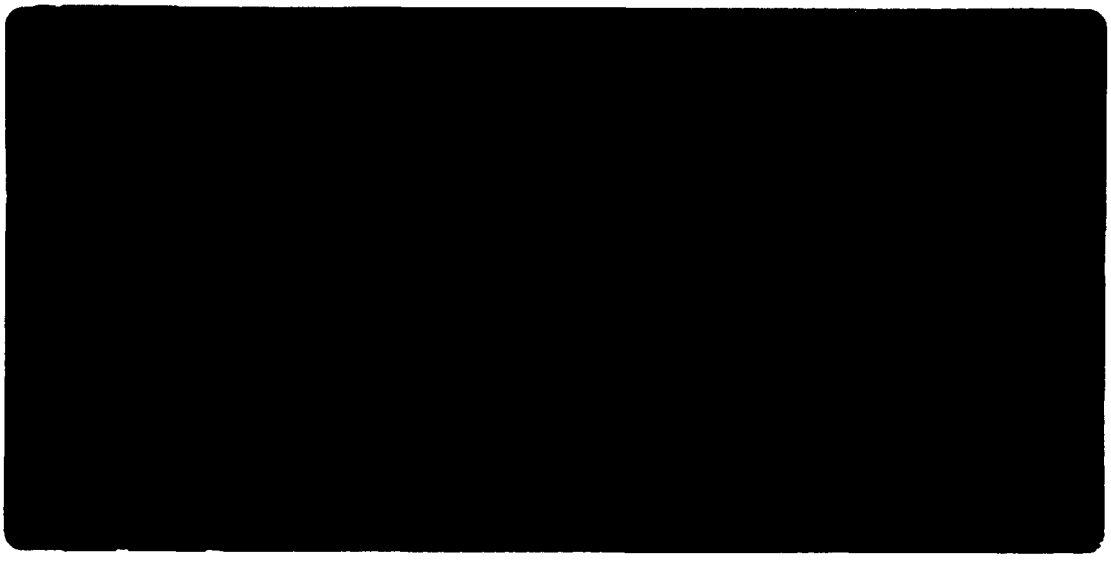

NUMBER 483

A COMPARISON OF CFD SIMULATIONS OF RECOVERY BOILER CHAR BEDS WITH 2-D AND 3-D GEOMETRIES

W. YANG, R.R. HORTON, AND T.N. ADAMS

APRIL 1993

A Comparison of CFD Simulations of Recovery Boiler Char Beds with 2-D and 3-D Geometries

W. Yang, R.R. Horton, and T.N. Adams

Submitted to
Tappi Journal

A COMPARISON OF CFD SIMULATIONS OF RECOVERY BOILER CHAR BEDS WITH 2-D AND 3-D GEOMETRIES

Wenrui Yang, Robert R. Horton, and Terry N. Adams

ABSTRACT

Char bed combustion is an integral part of the operation of recovery boilers. This paper presents results of several char bed CFD models of different geometries with particular emphasis on flow patterns and shear stress at the char bed surface. The geometries examined in this paper include two-dimensional (2-D) models that correspond to furnaces with long slot air ports on two opposing walls, three-dimensional (3-D) slab models that correspond to furnaces with individual air ports on two opposing walls, and a 3-D wedge model that resembles a furnace with air ports on all four walls. The effect of using a slot primary air port in a 3-D slab model is also examined.

The 2-D and 3-D models produce a generally similar trend: primary air jets have stronger impact on the char bed surface than secondary air jets because the primary air ports are closer to the bed surface than the secondary air ports. After impinging on the bed surface, the primary air jets diverge and dissipate quickly. The secondary air jets extend to the central region of the furnace and form an upward central core upon interacting with the opposing air jets. Significant differences have been found in results of different geometries. Two-dimensional models are generally not suitable for quantitative predictions of 3-D flow patterns because they cannot preserve all the 3-D features. However, a slot primary air port, which is 2-D in nature, may be used in a 3-D model for predicting overall flow patterns, especially for the middle and upper combustion zones because the influence of the primary air jets is restricted to a relatively small region near the primary air ports. The secondary air jet in the 3-D wedge model has little interaction with the char bed surface, whereas the secondaries in the slab models produce high shear stresses at the top of the bed where the jets impinge on the bed.

INTRODUCTION

Char bed combustion in a black liquor recovery boiler is a complicated process involving fluid flow, chemical reactions, and heat and mass transfer. Interaction between a char bed and air jets plays an important role in determining the shape of the bed and air flow pattern. Understanding char bed phenomena is important for stable furnace operation and improvement in furnace design. Unfortunately, little information is available about gas-char bed interaction since in an operating furnace, large dimensions and high temperatures make most measurements very difficult. Physical modelling is restricted to cold flows and cannot simulate the effect of gas flow patterns on char bed formation and development (1-4). Rapidly developing computational fluid dynamics (CFD) techniques provide a plausible means for research into this complicated char bed and flow interaction problem.

With advances in commercial CFD software, CFD techniques have become a powerful tool for research on complicated fluid flow problems. Applications of CFD methods in recovery furnace simulations have produced valuable information about flow patterns and interactions of air jets (4-12), interaction between black liquor spray and air flow (13), and heat and mass transfer and chemical reactions (6-8, 14-16). Simulation of char bed phenomena poses a greater challenge to CFD techniques. In addition to complicated transport and reaction processes, a char bed model involves a reacting boundary condition at the bed surface. The shape of the bed surface is determined by char arrival and consumption rates, which are not known beforehand. With this limitation, char bed simulations could only use assumed shapes in the boundary conditions (6, 16, 17).

Accurate simulation of char bed phenomena requires a CFD model to use large amounts of small computational cells to represent air ports and bed shape accurately. This is very difficult for a model that includes the entire combustion zone, because the required total number of nodes can easily exceed the maximum number allowed by software or computer memory. Within limits of software or hardware, whole furnace models with less than 200,000 cells could only use one cell for a primary air port, or a slot for all the primary air

ports (5-7, 15). These models are useful for predicting gas flow patterns in the middle or upper combustion zones, but they are not accurate enough for char bed studies. Symmetry planes have often been used to simplify furnace models and reduce computational burden (5, 8, 14, 16). By using symmetry planes, simulations can focus on a small section of a char bed to increase accuracy and numerical efficiency. When examining a small section of the overall flow problem, it is important to carefully impose boundaries and boundary conditions since they can influence simulation results.

To understand the effects of specifying boundary conditions on char bed simulations, we studied several simplified char bed models of different geometries. Gas velocity profiles and shear stress distributions on the bed surface were examined. The results provided important information in the selection of problem geometries for more complicated simulations.

In the next section, five char bed models of different geometries will be described in detail. Comparison of predicted velocity fields and shear stress distributions will be presented in the Results and Discussion section, followed by conclusions from this work.

DESCRIPTION OF CHAR BED MODELS

General Description of a Recovery Boiler Char Bed

In this study a typical, symmetrical furnace geometry is considered. The horizontal cross-section of the furnace is 10 m × 10 m. The primary air ports are 0.05 m wide and 0.3 m high, and are located on the walls at an elevation of 0.05 m with intervals of 0.3 m. The secondary air ports are 0.15 m wide and 0.5 m high, and are located on the walls at an elevation of 1.5 m with intervals of 1.5 m. Only the portion of the furnace below the liquor guns is considered. By using symmetry assumptions, the computational region is further reduced to a small section involving 2½ primary and one half secondary air ports, as is shown in Figure 1. The coordinate symbol indicates x, y, and z directions referred to in this

paper. The char bed surface starts to rise at 0.15 m from the wall with a 1:2 slope, and levels off at 3.7 m from the wall, resulting in a flat bed top of 1.775 m high. Part of the upper boundary is sloped to achieve efficient node distributions. The effect of such a sloped boundary on gas flow field is negligible since gas velocity is very low in this region. The inlet air velocities are assumed to be uniform at the air ports. The primary air velocity is 50 m/s in a 10° downward angle, the secondary air velocity is 80 m/s in the horizontal direction. This result in an average vertical velocity of 1.3 m/s in any horizontal cross-sectional plane above the secondary air port in the region shown in Figure 1. Heat transfer and chemical reactions are not considered in the present study, so an isothermal condition is assumed and the physical properties of air at 1000 °C are used.

Non-slip wall boundary conditions are used for the wall and the char bed. Fixed-velocity inlets are used for the air ports, and a fixed-pressure (isobaric) inlet is used for the upper boundary. The other boundaries of the slice are assumed to be symmetry planes. The standard κ-ϵ turbulent model is used.

The CFD code used in this work is FLUENT version 4.11 (18) with the capability of body-fitted-coordinate (BFC) grids (19). Unlike orthogonal Cartesian coordinate grids, which use steps to represent boundaries that do not align to the grid lines, BFC grid lines can be aligned to boundaries, regardless of their orientation, to form smooth boundaries. Internal grid lines can be arranged to follow major flow features to improve accuracy. The BFC grid not only increases the accuracy of the results, but also saves computational time by speeding up convergence (17). The CFD code was run on an IBM RISC/6000 computer.

Geometries of Char Bed Models

When simulating part of a furnace, imaginary planes that isolate the computational region from the rest of the furnace determine the shape of the char bed model. Five different geometries were examined in this study: two 2-D and three 3-D specifications.

1. Two-dimensional model number 1 (2D-1): This 2-D model neglects the variations in the z (thickness) direction, thus it corresponds to a furnace that has two infinitely long opposing walls with slot primary and secondary air ports. The slots maintain the heights of the original air ports, therefore, the primaries are enlarged six times and the secondaries are enlarged ten times in comparison with the 3-D rectangular air ports. Average vertical air velocity across the upper boundary increases from 1.3 m/s to 11 m/s correspondingly.

2. Two-dimensional model number 2 (2D-2): This 2-D model uses reduced air port sizes so that air velocities and overall flow rate can be maintained at realistic values. Both the primary and the secondary slot air ports have the same height of 0.05 m. This is equivalent to the 3-D rectangular air ports in area.

The grids of both 2-D models, 2D-1 and 2D-2, have the same number of cells ($67\times72=4824$), that are non-uniformly distributed to achieve higher resolutions near the air ports. By replacing the individual air ports with long slots, the characteristics of the air jets are changed. This will not only change the profiles of the jets but also eliminate the interactions between individual jets. Generally, 2-D models cannot maintain all the 3-D features, but their simplicity and fast convergent speed make them very useful in many situations.

3. Three-dimensional slab model number 1 (SLAB-1): This 3-D model follows the geometric features of the char bed illustrated in Figure 1. Two parallel symmetry planes on both sides of the slab imply that the slab pattern repeats as mirror images in the z direction *ad infinitum*. This is equivalent to a furnace with air ports on two infinitely long opposing walls. A non-uniform BFC grid with 149,544 ($67\times72\times31$) cells is specified to provide higher resolutions for the air jets. Figure 2 shows some surface nodes of the grid. A primary air port is represented by 36 (12×3) cells and the 1/2 secondary air port by 80 (16×5) cells.

4. Three-dimensional slab model number 2 (SLAB-2): This 3-D model has the same

geometric features as the SLAB-1 model except that the primary air ports are replaced by a slot of the same total area. A 3-D model can properly characterize the structure of a furnace, but it requires many more computational cells (31 times as many in the SLAB-1 model as in the 2-D models), thus considerably more memory and CPU time than a 2-D model. In the SLAB-1 model, significant number of cells are needed to resolve the primary air ports. Since the primary air ports are closely distributed in a narrow band near the bottom of the wall, the primary air jets may mix in a short distance, and their contribution to the overall flow field may resemble that of a planar slot jet. By using a slot primary air port, the number of cells in the SLAB-2 model is reduced to 101,128 ($67\times72\times22$) from 149,544 in the SLAB-1 model. This is a common practice in many 3-D recovery boiler simulations when the number of available cells is not enough to resolve the primary air ports (5, 6, 15). At the same elevation on the wall, the center of the slot air port is closer to the char bed surface than that of the rectangular air ports since the slot is shorter. The slot air port may cause errors to transport processes on the bed surface, which depend heavily on the flow patterns of the primary air jets.

5. Three-dimensional wedge model (WEDGE): For a furnace with air ports on four walls, parallel symmetry planes between adjacent air jets do not exist due to interactions between air jets from adjacent walls. An accurate simulation on the air jet interactions must include a larger computational region. To include some effects of the air jets from the adjacent walls while maintaining the reduced size of the model, one of the symmetry planes in the WEDGE model is angled slightly so that the two side planes meet at the center of the furnace to form a wedge-shaped geometry, as shown in Figure 3. As the air jets travel from the wall to the furnace center, the cross-sectional area reduces gradually to simulate the effect of the air jets from perpendicular side walls. Strictly speaking, the WEDGE model corresponds to a nearly circular furnace with uniformly distributed air ports around the wall. Air jets in the middle of a symmetrical square furnace may correspond to a situation between the slab and the wedge models. The WEDGE model has the same inlet air flow rate as the slab models, but its average vertical velocity at the upper boundary is twice as large due to smaller cross-sectional area.

All five models have the same number of cells in the x-y plane (67×72). Separate grid sensitivity studies have shown that current node density was adequate for grid-independent solutions in nearly the entire computational region. However, turbulent kinetic energy and eddy dissipation rate were found to be grid-sensitive in very small regions at the edges of the air jet entrances. This was not due to inadequate node density in those regions, but rather to the uniform inlet velocities that resulted in velocity discontinuity at the edges of the entering air jets. More practical velocity profiles should be used in the inlet boundary conditions to overcome this problem. In the present study, the effect of the velocity discontinuity is negligible.

The SLAB-1 and WEDGE models have the same number of cells in the z direction (31 cells). Such a node density is more than enough to achieve grid-independent solutions in almost the entire simulation zone except a small region near the primary air ports where the solutions are slightly grid-sensitive due to abrupt velocity variations in the z direction. The quadratic up wind interpolation (QUICK) scheme (18) is used in this study to minimize numerical diffusion errors that may occur to jet flows not aligned with the grid lines.

RESULTS AND DISCUSSION

Gas Flow Predictions

Distributions of velocity magnitude for the 2-D models are shown in Figures 4 and 5. The gray scale ranges from 0 m/s in the darkest areas to 80 m/s in the brightest areas. The same gray scale is used for all other velocity distribution patterns in this paper. Model 2D-1 predicts very strong air jets because of the large slot air ports. The primary air jet extends a long distance along the char bed surface and merges with the secondary air jet near the top of the bed. The secondary jet curves upward gradually due to its interaction with the primary jet, the rising bed surface, and the opposing secondary jet.

In comparison, model 2D-2 with adjusted air port sizes predicts much thinner and

weaker air jets. The primary jet has almost dissipated before it meets the secondary jet. The secondary jet is so weak that it is pulled downward by a low pressure region below it. As a result, the secondary air has greater contact with the char bed than in model 2D-1. This may affect computation of transport processes on the bed surface. The streamlines in Figures 6 and 7 show structures of the jet streams and recirculations. Two opposite recirculation zones exist between the primary and secondary jets, and a large recirculation zone above the secondary jet, causing a slow downward flow near the wall.

Figure 8 shows the velocity distribution pattern of the 3-D SLAB-1 model at three boundaries of the model. Unlike the 2-D secondary air jets, which change directions shortly after entering the furnace, the 3-D secondary air jet penetrates horizontally into the furnace to the bed surface. The 3-D primary jets dissipate quickly after impinging on the bed surface. There is little direct interaction between the primary and the secondary jets, but interaction between primary jets is strong since they are very close and are deflected by the bed surface. Figure 9 shows velocity distributions on a series of cross-sections of the slab. The secondary jet expands and dissipates towards the center. The primary jets are deflected by the bed surface and then adjacent jets interact with each other to form new streams between the air jets. This process consumes kinetic energy and increases dissipation. After a distance of about one meter, the primary jets are well mixed as if the air came from a planar jet.

Figure 10 shows the flow pattern of the modified slab model, SLAB-2. The secondary air jet is the same as that of the original model, SLAB-1. The planar primary air jet does not undergo the interaction processes that occur with individual rectangular air jets, thus the planar jet dissipates slower and travels further than the rectangular jets. Similar to the case with individual jets, the planar primary air jet has little effect on the secondary air jet. The major flow patterns of both models are very similar. This suggests that the slot primary air port may be suitable for predicting overall flow patterns, especially those focusing on the middle and upper combustion zones in the furnace.

The velocity distribution for the WEDGE model is shown in Figure 11. The primary air jets dissipate in a short distance after impinging on the bed surface. Within this distance (1/3 of the furnace depth), the effect of the wedge shape is small, and both the primary and part of the secondary air jets resemble those of the SLAB-1 model. At about half the distance to the center of the furnace, the converging side boundaries force the secondary air to turn upward before the main stream of the jet reaches the bed surface, resulting in a strong upwardly directed flow at the furnace center. At the edge of the flat top of the char bed, the secondary air stream separates from the bed surface, creating a recirculation zone above the bed top. This is different from the predictions of the slab models, where the recirculation zones above the bed top are negligibly small.

The high velocity central core may play an important part in particle entrainment and carryover (15). Figure 12 compares the average vertical velocities at the upper boundary. A common feature of the models is that they all predict highest velocities in the center, which is inevitable for symmetrical air port distributions. Model 2D-1 predicts unrealistically high velocity due to the large slot air ports. The other four models have the same total air flow rate. The WEDGE model predicts higher velocities than the slab models because it has less cross-sectional area and the converging side symmetry planes force the air jet to turn upward sooner. It is interesting that the slab models and the 2D-2 model predict similar velocity distributions at the upper boundary. The differences caused by the air port shapes gradually disappear as the air jets expand and mix. If the flow pattern of the primary air jets is not a major concern, using a slot primary air port configuration can save memory and computational time.

Interaction of Air Jets with Bed Surface

Shear stress on the bed surface indicates the rate of momentum transfer, which is analogous to heat and mass transfer (16, 21). Since the char bed combustion rate can be mass transfer limited (22), the shear stress distribution has important implications for understanding the char bed phenomena. Higher shear stress indicates greater heat and mass

transfer rates and, therefore, faster char combustion. Although the shape of the primary air ports does not have significant influence on the overall gas flow pattern, it affects gas flow near the bed surface and shear stress distribution. The shear stress on the bed surface is calculated from the near-wall velocity and turbulent kinetic energy using the log-law wall function (18, 20).

Figure 13 shows plan views of shear stress distributions on the bed surface. The 2-D models have been extended in the z direction to show the bed surface. The gray scales range from 0 Pa in the darkest areas to 2.8 Pa for Figure 13(a), and 1.5 Pa for Figures 13(b), (c), (d), and (e) in the brightest areas. The maximum shear stress is produced by the impingement of the primary air jets because they are very close to the bed. The shear stress produced by a planar jet is uniform in the z direction. A rectangular primary jet in the 3-D models produces a high shear stress area that is much wider than the air port due to expansion of the air jet on the bed surface.

The effects of the secondary jets depend on the contact of the jets with the bed surface. In the WEDGE model, the main stream of the secondary jet does not touch the bed; therefore, its contribution to the shear stress is very small. In comparison, the secondary jets in the two slab models produce areas of high shear stress at the top of the bed where the air jets impinge on the bed surface.

The shear stress distributions, averaged in the z direction, are compared quantitatively in Figure 14. The primary air jets produce comparable shear stresses with the same air flow rate and initial velocity, except that of the 2D-1 model. The planar jets produce slightly higher average shear stresses than the rectangular jets because the centers of the planar jets are closer to the bed surface. Model 2D-2 produces higher shear stress in the middle of the bed than other similar cases because the secondary jet bends down and contacts the bed surface earlier. There is a large difference between the contributions of the secondary jets of the WEDGE model and the slab models. In the WEDGE model, since the secondary jet turns away from the bed, the shear stress on the upper part of the bed is much smaller than

that in the slab models.

The turbulent boundary layer theory shows that turbulent kinetic energy near a surface is also a determining factor for transport processes (20). The distribution patterns of turbulent kinetic energy shown in Figure 15 are very similar to those of shear stress in Figure 14. The rectangular primary jets are more turbulent initially but decay faster than the planar jets because they expand rapidly and impact against each other after impinging on the bed surface. The results indicate that geometry of primary air ports does affect heat and mass transfer processes on the bed surface.

Although the predicted velocity fields and shear stress distributions are related to the specific char bed geometries, there are still some common principles that are applicable to other char bed structures. Both the shear stress and the turbulent kinetic energy distributions indicate that the primary air jets are always important for the transport processes on the bed surface; however, the effects are limited to the base of the bed. The effects of the secondary air jets depend on whether they impinge on the bed surface. For a tall char bed that grows above the secondary jets, the secondary air may contribute significantly to the combustion at the top of the bed. If the bed is well below the secondary air jets, the secondaries may not have any interaction with the bed.

CONCLUSIONS

CFD simulations with five different geometries for recovery furnace char beds are presented in this paper. The following conclusions can be drawn from the results.

Two-dimensional models are not suitable for predicting gas flow patterns quantitatively because they can not preserve all the three dimensional features of real furnaces.

Geometry of primary air ports has little effect on the flow pattern of a secondary air

jet, thus a planar primary air jet in a 3-D model may be acceptable for predicting flow patterns in the middle and upper combustion zones.

The slab models are suitable for furnaces with air jets on two opposing walls, whereas the WEDGE model can include some effect of air jets from perpendicular side walls. More accurate simulations for interaction of perpendicular air jets must be carried out in larger regions involving two adjacent walls.

For the bed shape considered in this paper, primary air jets produce higher shear stress on a bed surface than secondary air jets, therefore, the primary air jets may be more important in controlling bed shape. Geometries of air ports affect shear stress distributions, as well as distributions of turbulent kinetic energy. This means that they also affect mass transfer process, which may be the rate-limiting step for char bed combustion.

ACKNOWLEDGMENT

This work was supported by DOE under contract No. DE-FG02-90CE40936.

REFERENCES

1. Blackwell, B., "Validity of Physical Flow Modeling of Kraft Recovery Boilers," *Tappi J.* **75**(9), 122 (1992).

2. Ketler, S. P., Savage, M. C., and Gartshore, I. S., "Physical Modeling of Flow in Black Liquor Recovery Boilers," *Proc. TAPPI Eng. Conf.*, p. 581, 1992.

3. Llinares, V. Jr. and Chapman, P. J., "Combustion Engineering Update Stationary Firing, Three Level Air System Retrofit Experience," *Proc. TAPPI Eng. Conf.*, p. 629, 1989.

4. Chapman, P. J. and Jones, A. K., "Recovery Boiler Secondary Air System Development Using Experimental and Computational Fluid Dynamics," *Proc. TAPPI Eng. Conf.*, p. 193, 1990.

5. Jones, A. K. and Grace T. M., "A Comparison of Computational and Experimental Methods for Determining the Gas Flow Patterns in the Kraft Recovery Boiler," *Proc. TAPPI Eng. Conf.*, p. 3, 1988.

6. Sumnicht, D. W., "A Computer Model of a Kraft Char Bed," Ph.D. Thesis, IPC, April, 1989.

7. Chapman, P. J. and Jones, A. K., "Recovery Furnace Combustion Modeling Using Computational Fluid Dynamics," *Proc. Int'l Chem. Recovery Conf.*, p. 71, 1992.

8. Vakkilainen, E. K., Adams, T. N., and Horton, R. R., "The Effect of Recovery Furnace Bullnose Designs on Upper Furnace Flow and Temperature Profiles," *Proc. Int'l Chem. Recovery Conf.*, p. 101, 1992.

9. Siiskonen, P., Karvinen, R., Hyoty, P., Migaj, V. K., and Morgoun, A. V., "Combined Physical and Numerical Study of a Multilevel Air System," *Proc. Int'l Chem. Recovery Conf.*, p. 57, 1992.

10. Salcudean, M., Nowak, P., and Abdullah, Z., "Mathematical Modeling of Recovery Furnaces," *Proc. Int'l Chem. Recovery Conf.*, p. 197, 1992.

11. Abdullah, Z., Nowak, P., Salcudean, M., and Gartshore, I. S., "Investigation of Interlaced and Opposed Jet Arrangements for Recovery Furnaces," *Proc. TAPPI Eng. Conf.*, p. 103, 1992.

12. Quick, J. W., Gartshore, I. S., and Salcudean, M., "Interaction of Opposing Jets With Special Relevance to Recovery Furnaces," *Proc. TAPPI Eng. Conf.*, p. 123, 1992.

13. Adams, T. N. and Horton, R. R., "The Effects of Black Liquor Spray on Gas Phase Flows in a Recovery Boiler," *Proc. TAPPI Eng. Conf.*, p. 81, 1992.

14. Karvinen, R., Hyoty, P., and Siiskonen, P., "The Effect of Dry Solids Contents on Recovery Boiler Furnace Behavior," *Tappi J.* 74(12), 171(1991).

15. Horton, R. R., Grace, T. M., and Adams, T. N., "The Effects of Black Liquor Spray Parameters on Combustion Behavior in Recovery Furnace Simulations," *Proc. Int'l Chem. Recovery Conf.*, p. 85, 1992.

16. Sutinen, J. E. and Karvinen, R., "Numerical Modeling of Char Bed Phenomena," *Proc. Int'l Chem. Recovery Conf.*, p. 79, 1992.

17. Yang, W., Horton, R. R., and Adams, T. N., "CFD Simulations of Recovery Boiler Char Beds with Step and Smooth Surfaces," to be published.

18. FLUENT User's Guide, Ver. 4.0, Fluent Inc., December 1991.

19. PreBFC User's Guide, Ver. 4.0, Fluent Inc., December 1991.

20. Launder, B. E. and Spalding, D. B., *The Numerical Computation of Turbulent Flows*, Imperial College of Science and Technology, London, Jan., 1973.

21. Incropera, F. P. and De Witt, D. P., *Fundamentals of Heat and Mass Transfer*, 2nd ed., John Willey & Sons, New York, 1985.

22. Grace, T. M., Lien, S. J., and Brown, C. A., "Char Bed Burning - Laboratory Studies," *Proc. Int'l Chem. Recovery Conf.*, p. 539, 1992.

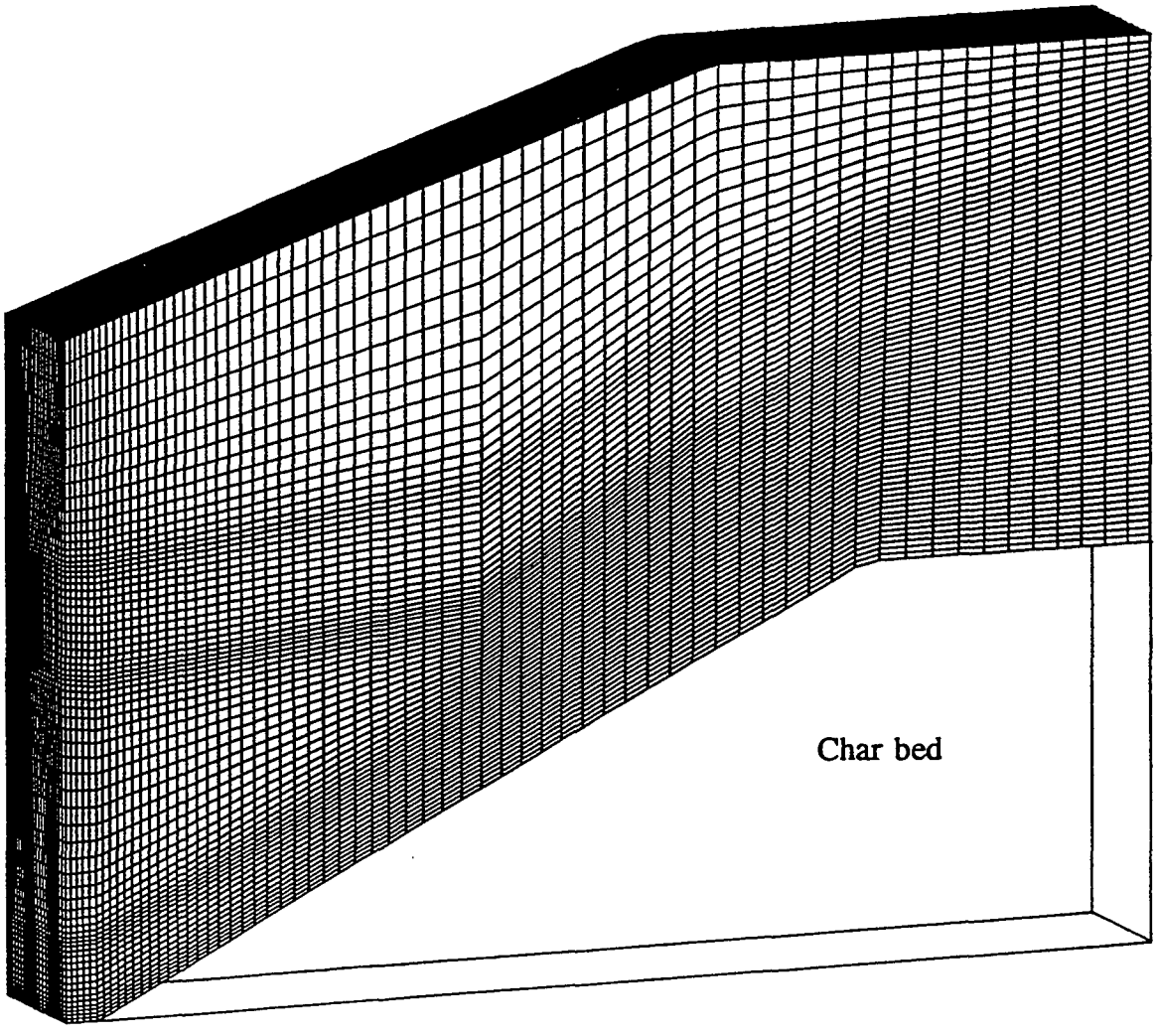

Figure 2. A non-uniform BFC grid for the SLAB-1 model.

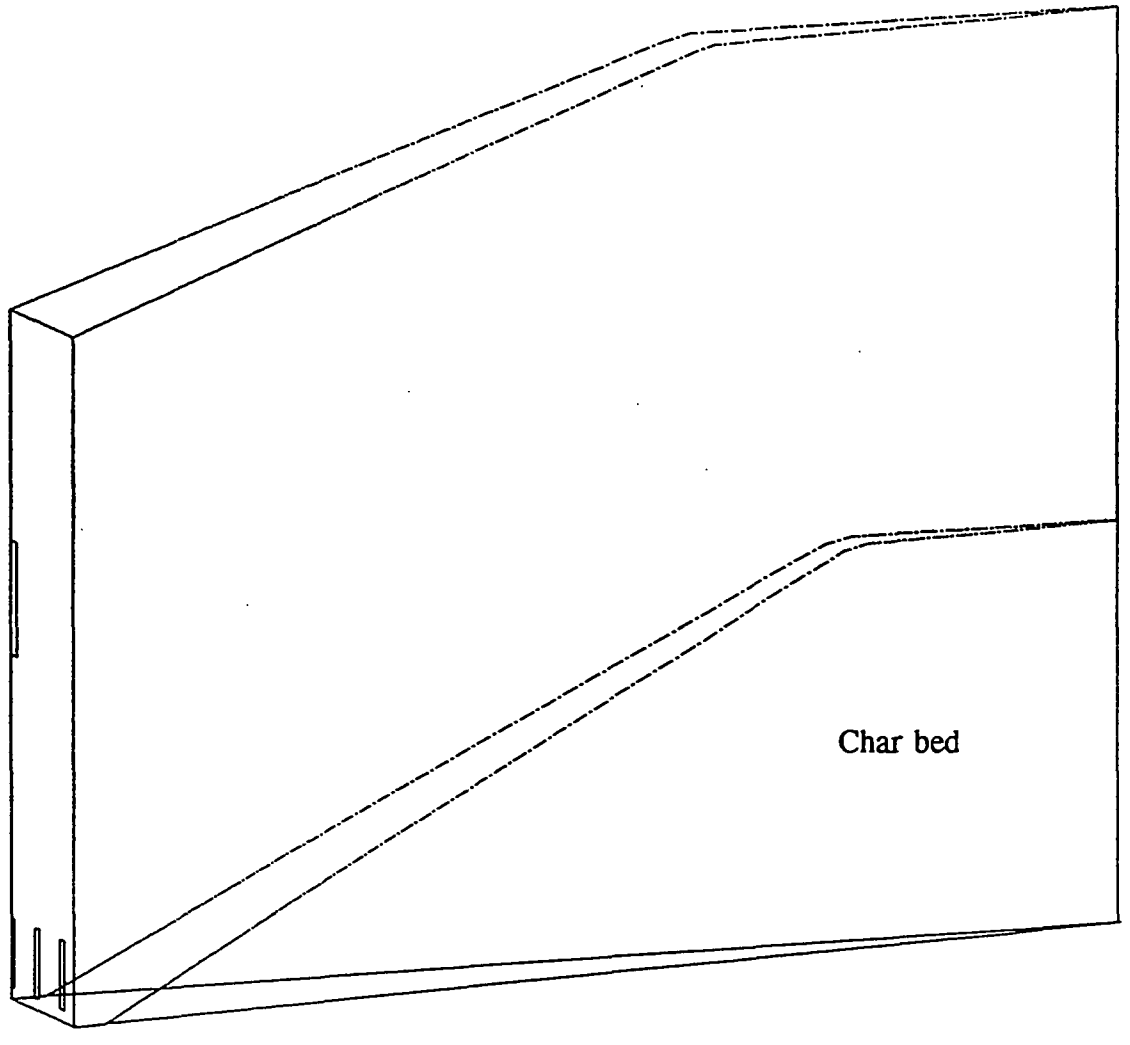

Figure 3. Geometry of the WEDGE model.

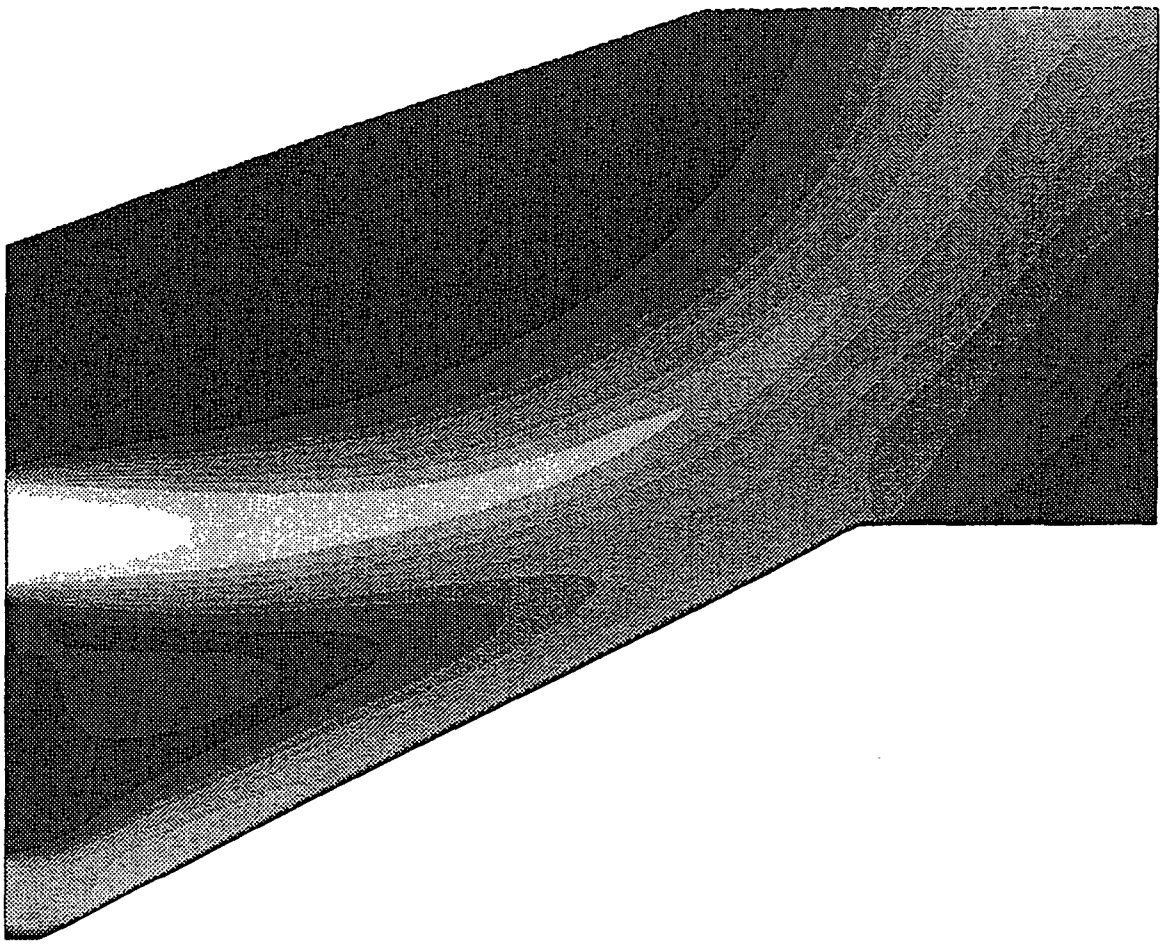

Figure 4. Velocity magnitude distribution for the 2D-1 model.

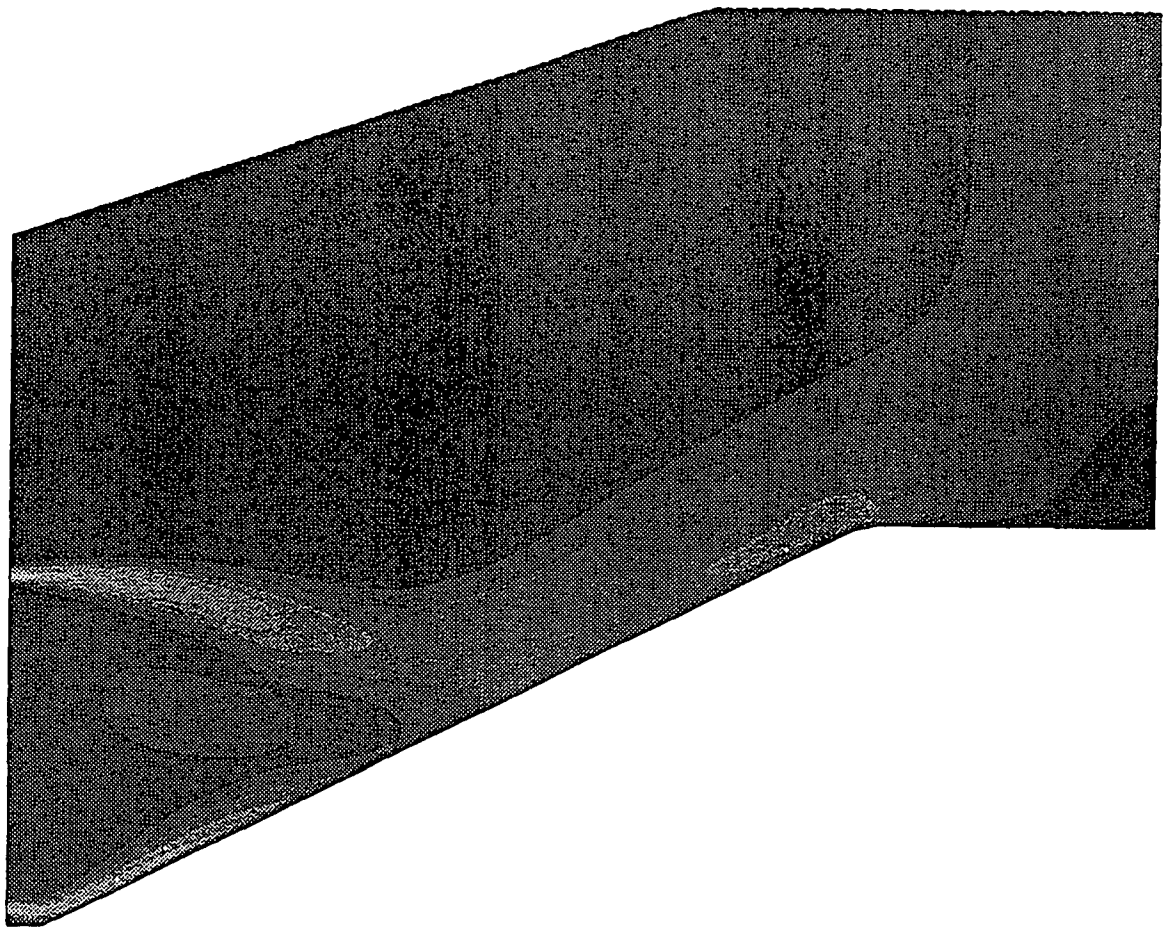

Figure 5. Velocity magnitude distribution for the 2D-2 model.

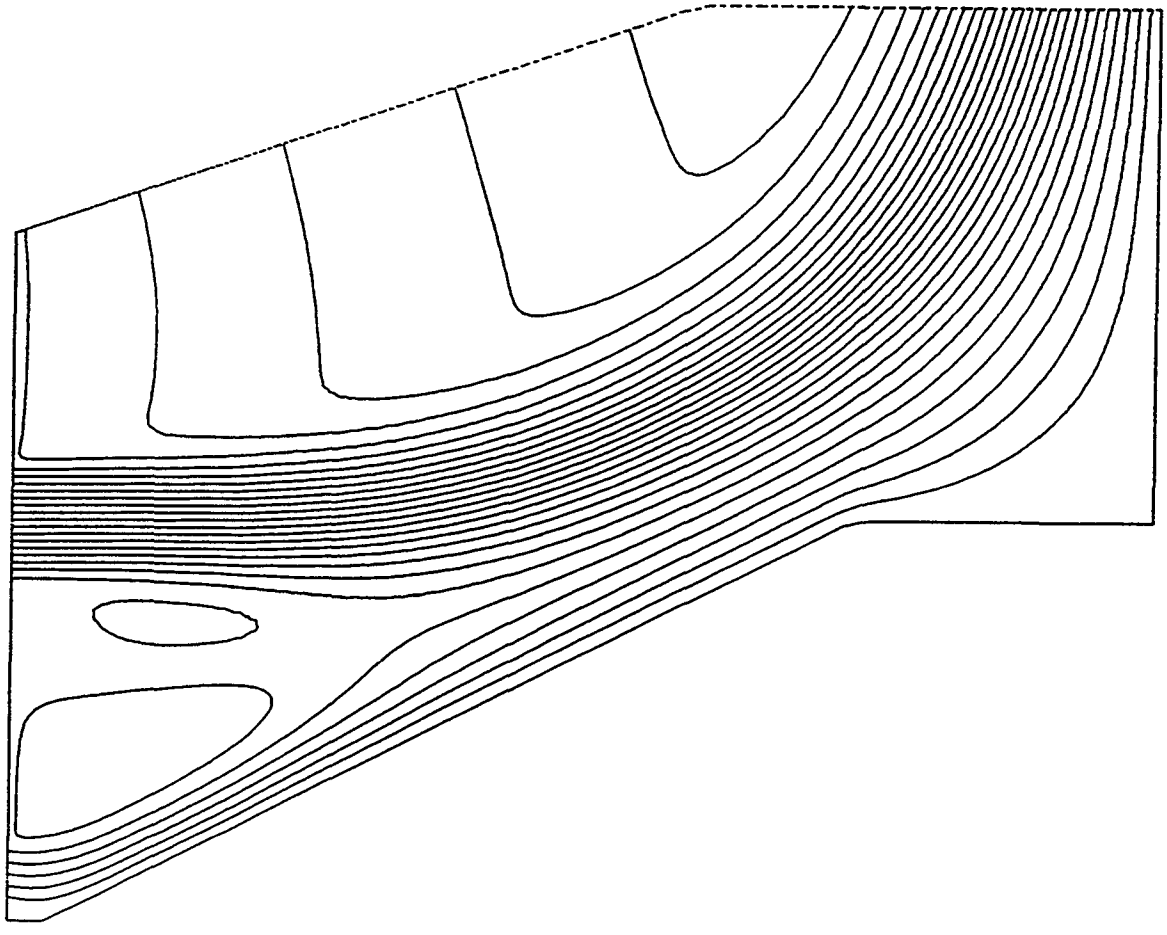

Figure 6. Streamlines for the 2D-1 model.

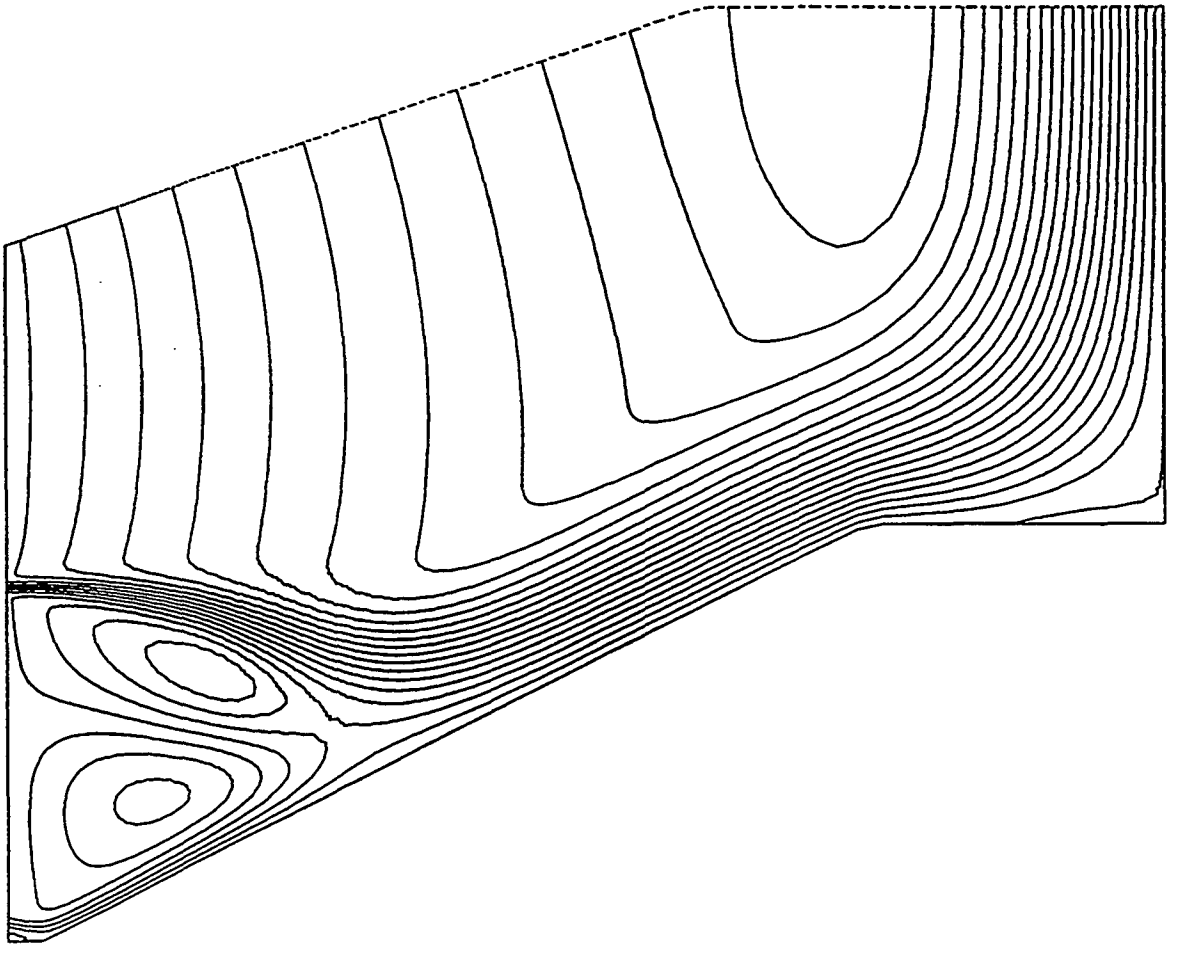

Figure 7. Streamlines for the 2D-2 model.

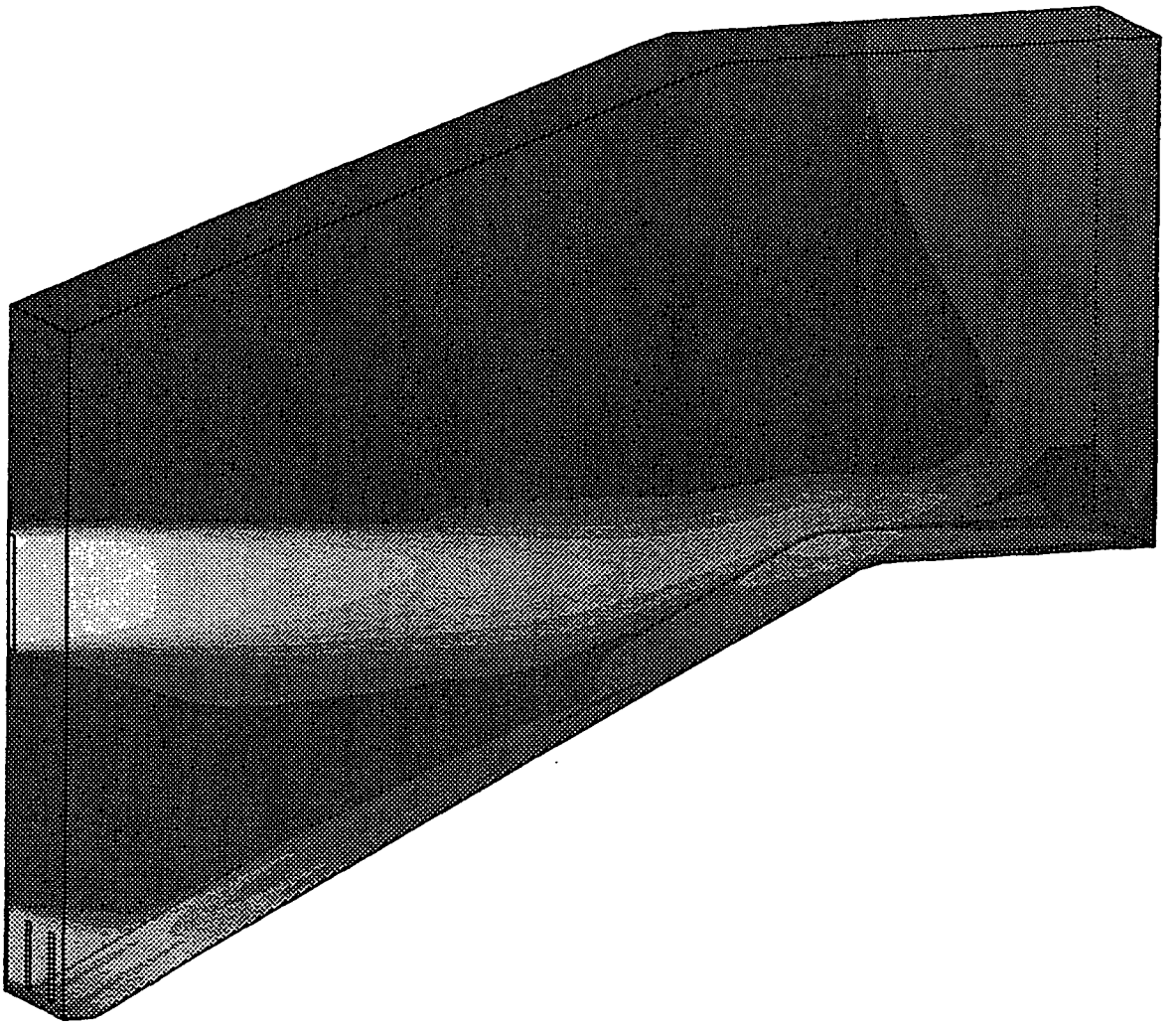

Figure 8. Velocity magnitude distribution for the SLAB-1 model on three boundaries.

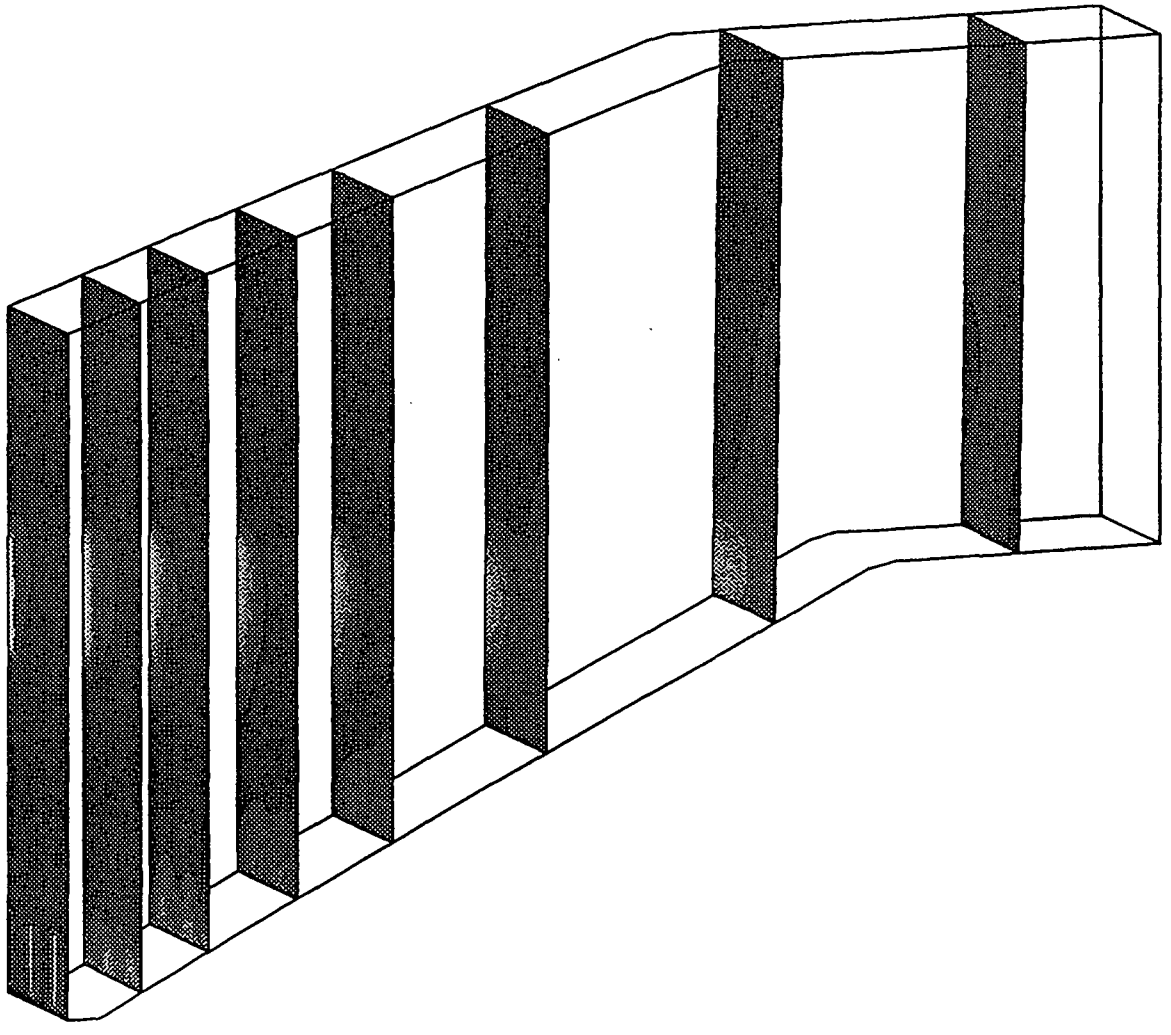

Figure 9. Velocity magnitude distribution for the SLAB-1 model on a series of cross-sectional planes.

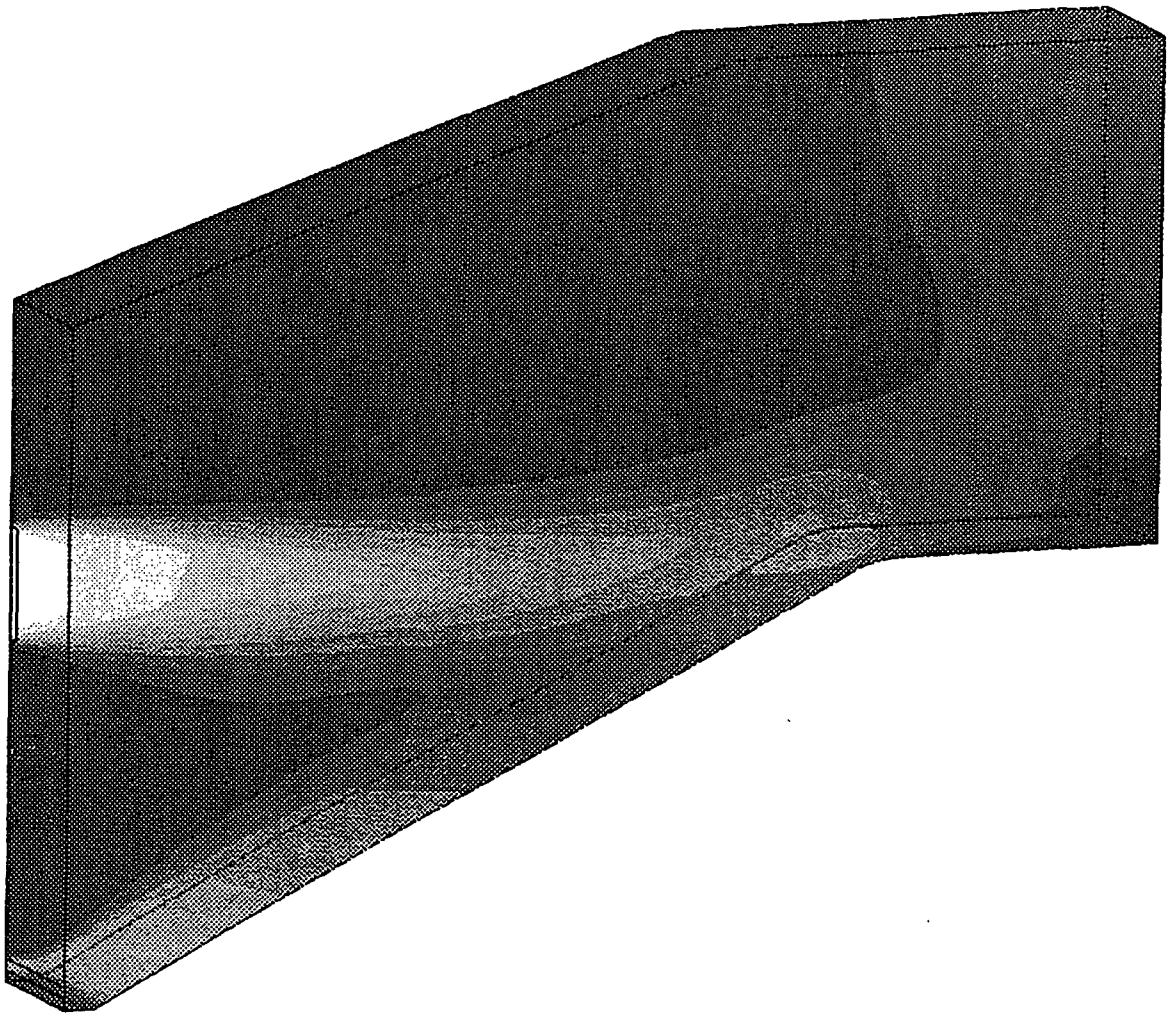

Figure 10. Velocity magnitude distribution for the SLAB-2 model on three boundaries.

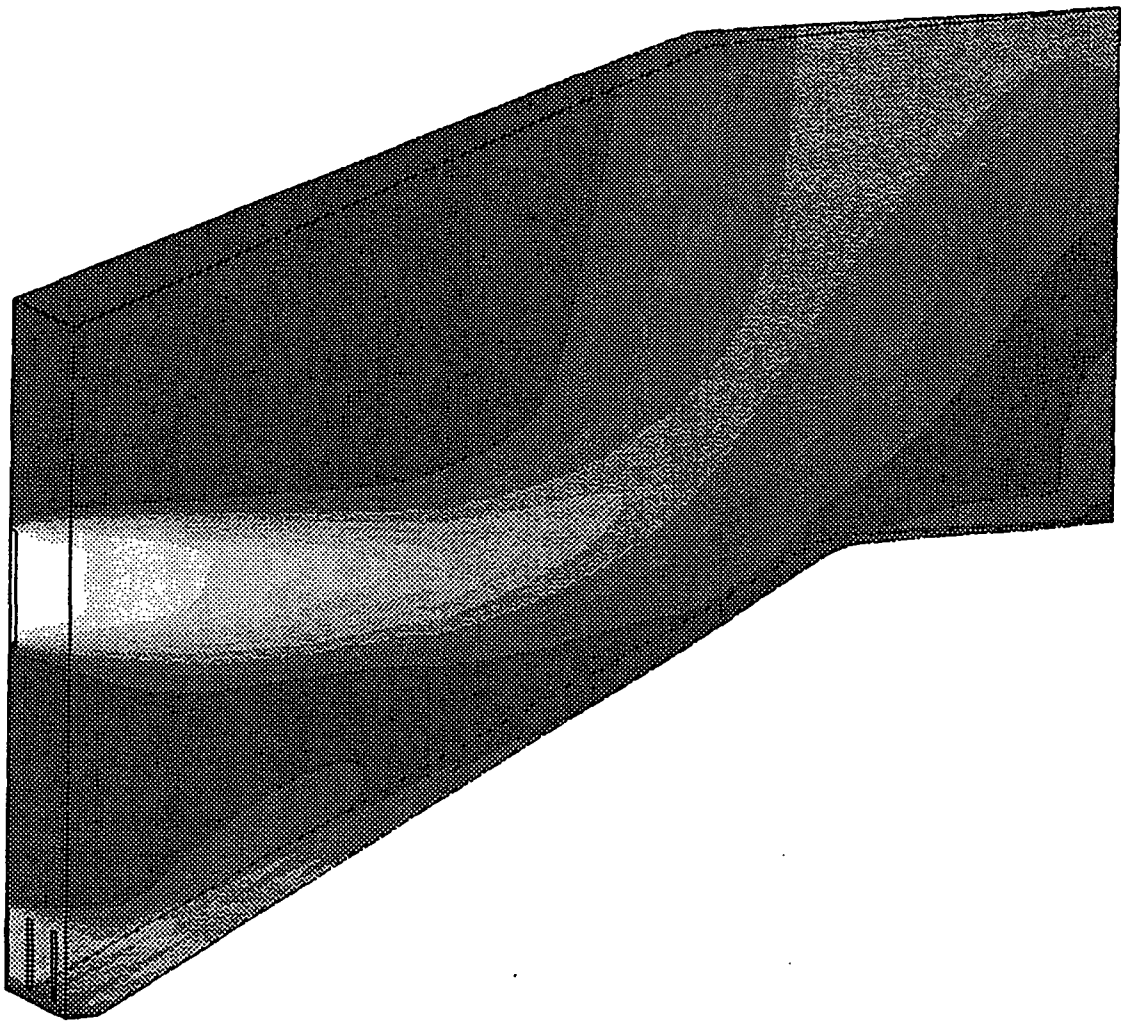

Figure 11. Velocity magnitude distribution for the WEDGE model on two boundaries.

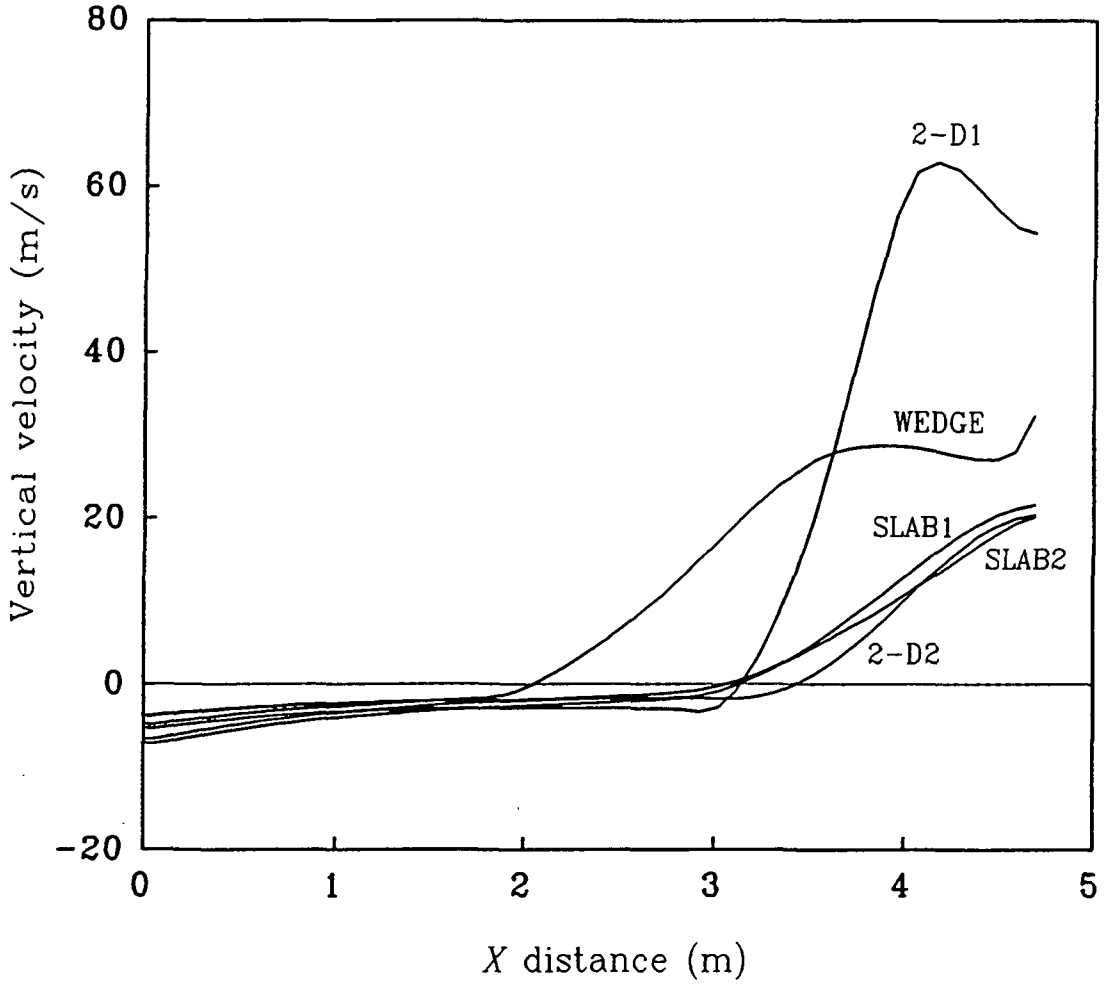

Figure 12. Comparison of average vertical velocities at the upper boundary.

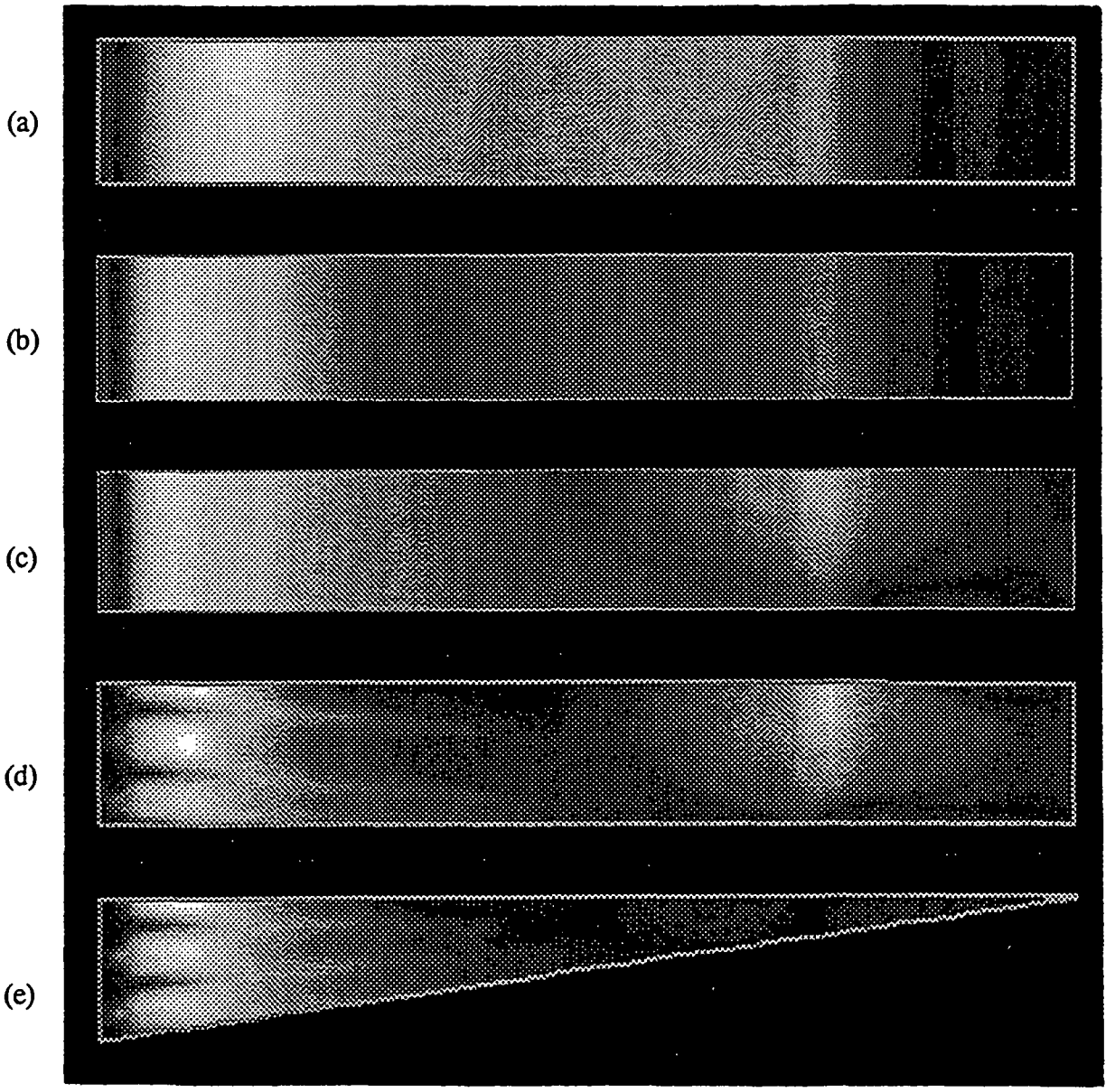

Figure 13. Patterns of shear stress distributions on the char bed surface.
(a) 2D-1, (b) 2D-2, (c) SLAB-2, (d) SLAB-1, (e) WEDGE.

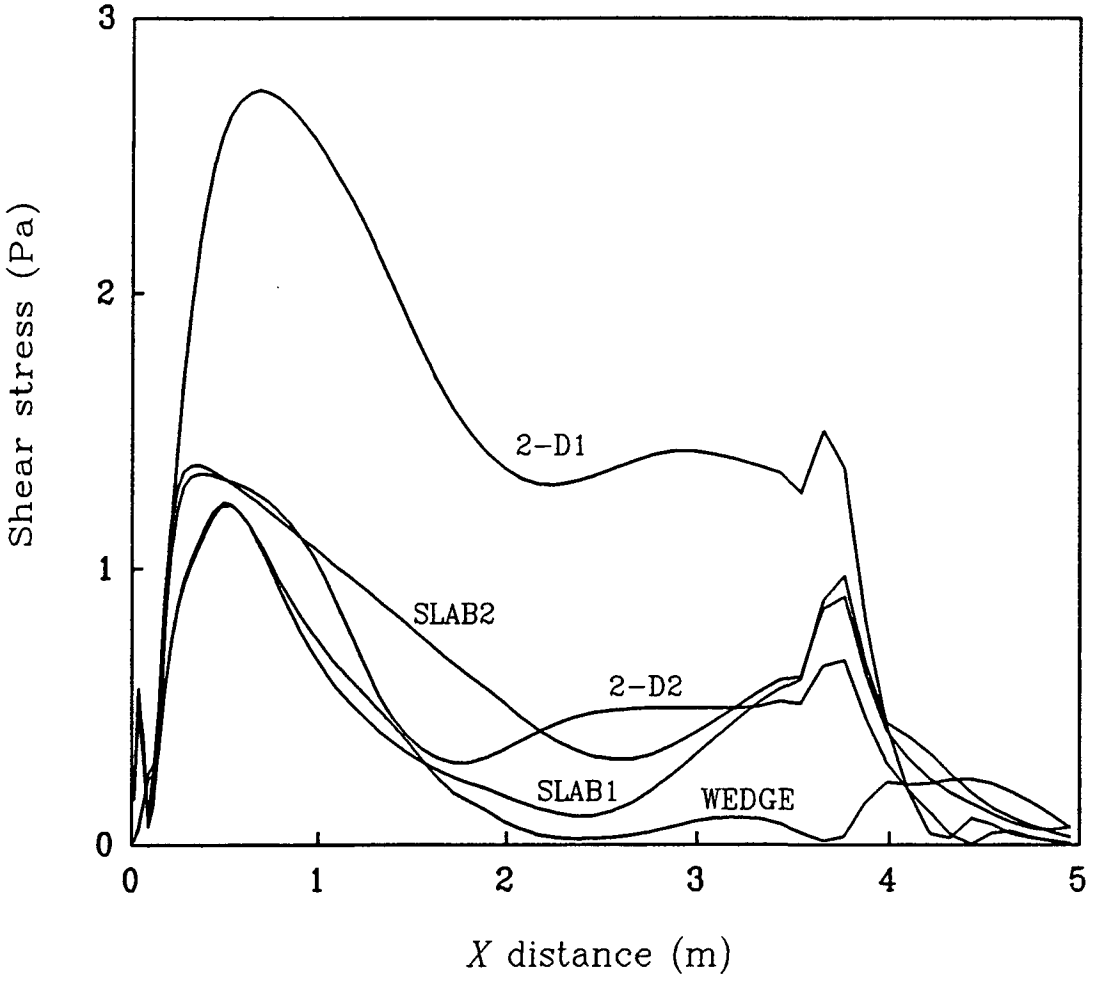

Figure 14. Comparison of average shear stress distributions on the bed surface.

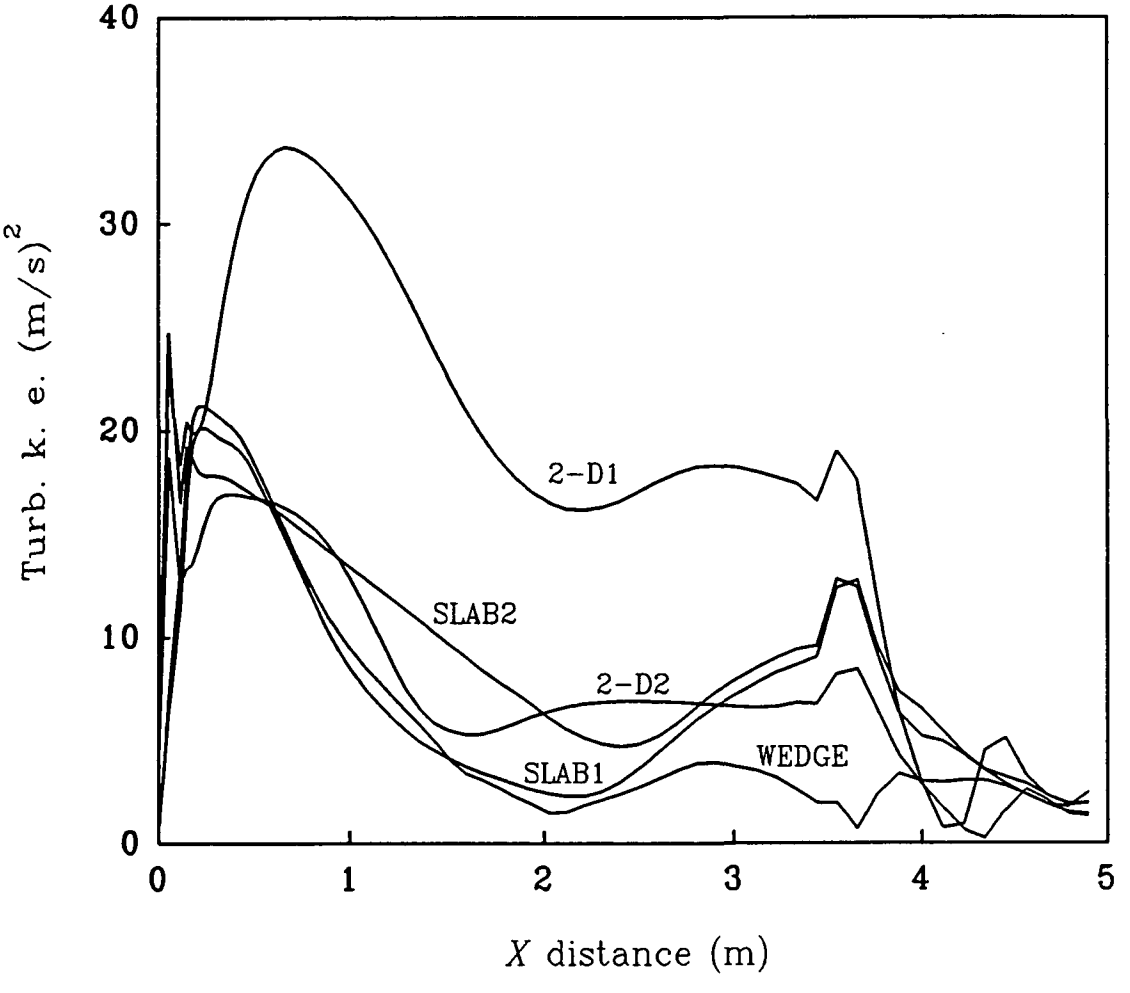

Figure 15. Comparison of average turbulent kinetic energy distributions on the bed surface.